

THE NASA-UC ETA-EARTH PROGRAM: II. A PLANET ORBITING HD 156668 WITH A MINIMUM MASS OF FOUR EARTH MASSES¹

ANDREW W. HOWARD^{2,3}, JOHN ASHER JOHNSON⁴, GEOFFREY W. MARCY², DEBRA A. FISCHER⁵,
JASON T. WRIGHT⁶, GREGORY W. HENRY⁷, HOWARD ISAACSON²,
JEFF A. VALENTI⁸, JAY ANDERSON⁸, AND NIKOLAI E. PISKUNOV⁹,

Submitted to ApJ

ABSTRACT

We report the discovery of HD 156668 b, an extrasolar planet with a minimum mass of $M_P \sin i = 4.15 M_\oplus$. This planet was discovered through Keplerian modeling of precise radial velocities from Keck-HIRES and is the second super-Earth to emerge from the NASA-UC Eta-Earth Survey. The best-fit orbit is consistent with circular and has a period of $P = 4.6455$ d. The Doppler semi-amplitude of this planet, $K = 1.89 \text{ m s}^{-1}$, is among the lowest ever detected, on par with the detection of GJ 581 e using HARPS. A longer period ($P \approx 2.3$ yr), low-amplitude signal of unknown origin was also detected in the radial velocities and was filtered out of the data while fitting the short-period planet. Additional data are required to determine if the long-period signal is due to a second planet, stellar activity, or another source. Photometric observations using the Automated Photometric Telescopes at Fairborn Observatory show that HD 156668 (an old, quiet K3 dwarf) is photometrically constant over the radial velocity period to 0.1 mmag, supporting the existence of the planet. No transits were detected down to a photometric limit of ~ 3 mmag, ruling out transiting planets dominated by extremely bloated atmospheres, but not precluding a transiting solid/liquid planet with a modest atmosphere.

Subject headings: planetary systems — stars: individual (HD 156668) — techniques: radial velocity

1. INTRODUCTION

The search for low-mass planets is driven by a desire to observationally study the full range of planetary systems in order to better understand their formation, dynamics, composition, and diversity. We also seek Earth-like worlds of terrestrial composition as a goal in itself and as targets for future transit and imaging observations. This search has taken several leaps forward recently because of instrumental improvements. The precision of radial velocity (RV) measurements with Keck-HIRES by the California Planet Survey (CPS) group (Howard et al. 2009b), HARPS (Lovis et al. 2006), and the AAT (O’Toole et al. 2009) has now reached 1 m s^{-1} or better and has led to the discovery of several super-Earths around nearby, bright stars. Ground-based transit surveys such as MEarth (Charbonneau et al. 2009) and HATNet (Bakos et al.

2009) have made important discoveries of transiting low-mass planets. Microlensing searches have detected two super-Earths orbiting distant stars (Beaulieu et al. 2006; Bennett et al. 2008) and the statistics of microlensing detections suggest that cold Neptunes are a factor of three more common than cold Jupiters (Sumi et al. 2009). From space, *CoRoT* has found a system with two super-Earths (one of which transits; Léger et al. 2009) and *Kepler* is poised to detect true Earth analogues in 1 AU orbits using transit photometry with a precision of 20 ppm in 6.5 hr (Borucki et al. 2009). In the next decade, *SIM Lite* (Unwin et al. 2008) will astrometrically characterize essentially all planets down to Earth mass orbiting ~ 100 nearby stars, as well as the more massive planets orbiting ~ 1000 stars.

The Eta-Earth Survey plays a unique role in the study of low-mass exoplanets. The population of 230 GKM stars in the survey is nearly free of statistical bias since the stars were not chosen based on their likelihood of harboring a planet, but rather on proximity, brightness, and chromospheric activity. Each star is observed at least 20 times, insuring a minimum detectability threshold. Thus, the distributions of planet detections and non-detections from the Eta-Earth Survey will yield a wealth of information about the efficiency and mechanisms of planet formation as well as the range of subsequent dynamical histories. The 20 survey observations per Eta-Earth Survey target are nearly complete and we are aggressively re-observing several promising candidate low-mass planets.

Current theories of planet formation (Ida & Lin 2004; Mordasini et al. 2009) are consistent with the measured distributions of massive planets (Saturn mass and above), but their predictions for the abundance and properties of low-mass planets are only now being observa-

¹ Based on observations obtained at the W.M. Keck Observatory, which is operated jointly by the University of California and the California Institute of Technology. Keck time has been granted by both NASA and the University of California.

² Department of Astronomy, University of California, Berkeley, CA 94720-3411, USA

³ Townes Fellow, Space Sciences Laboratory, University of California, Berkeley, CA 94720-7450 USA; howard@astro.berkeley.edu

⁴ Department of Astrophysics, California Institute of Technology, MC 249-17, Pasadena, CA 91125, USA

⁵ Department of Astronomy, Yale University, New Haven, CT 06511, USA

⁶ The Pennsylvania State University, University Park, PA 16802

⁷ Center of Excellence in Information Systems, Tennessee State University, 3500 John A. Merritt Blvd., Box 9501, Nashville, TN 37209, USA

⁸ Space Telescope Science Institute, 3700 San Martin Dr., Baltimore, MD 21218, USA

⁹ Department of Astronomy and Space Physics, Uppsala University, Box 515, 751 20 Uppsala, Sweden

TABLE 1
STELLAR PROPERTIES OF HD 156668

Parameter	Value
Spectral type	K3 V
M_V	6.480
$B - V$	1.015
V	8.424
J	6.593
H	6.117
K	6.004
Distance (pc)	24.5 ± 0.5
[Fe/H]	$+0.05 \pm 0.06$
T_{eff} (K)	4850 ± 88
$v \sin i$ (km s $^{-1}$)	0.50 ± 1.0
$\log g$	4.598 ± 0.12
L_* (L_\odot)	0.230 ± 0.018
M_* (M_\odot)	0.772 ± 0.020
R_* (R_\odot)	0.720 ± 0.013
Age (Gyr)	8.6 ± 4.8
$\log R'_{\text{HK}}$	-4.98
S_{HK}	0.23
P_{rot} (days)	51.5
σ_{phot} (mag)	$\lesssim 0.002$

tionally tested. In particular, they predict a dearth of planets below roughly Saturn mass in orbits inside the ice line. Such planets are predicted to be rare because once a planet core grows by planetesimal accretion to a of threshold mass of $\sim 10 M_\oplus$, it undergoes runaway gas accretion and becomes a gas giant. While these theories consistently predict such a “planet desert”, they differ in the contours of the desert in M and a as well as whether the planets below the critical core mass survive Type I inward migration in significant numbers.

In this context we announce the discovery of HD 156668 b, a super-Earth planet with minimum mass $M_P \sin i = 4.15 M_\oplus$ and an orbital period of $P = 4.6455$ d. This is the second super-Earth ($M \sin i < 10 M_\oplus$) to emerge from Keck observations explicitly for the NASA-UC Eta-Earth Survey, the first being HD 7924 b (Howard et al. 2009b). The remainder of this paper is structured as follows. We describe the host star properties in § 2. The spectroscopic observations and their Doppler reduction are described in § 3. In § 4, we describe the detection of the $P = 4.6455$ d orbit of HD 156668 b, and the high-pass filtering of the RV data that was necessary to obtain good estimates of the orbital parameters. In § 5 we carefully consider the null hypothesis—the non-existence of HD 156668 b—using S_{HK} measurements, photometric observations, and FAP analyses. We summarize and discuss the implications of this discovery in § 6.

2. STELLAR PROPERTIES

HD 156668 (HIP 84607) is a K3 dwarf (Gray et al. 2003) whose properties are summarized in Table 1. It is nearby ($d = 24.5$ pc; van Leeuwen 2007) and relatively bright ($V = 8.424$; Høg et al. 2000). With $M_V = 6.480$ and $B - V = 1.015$, the star lies near the *Hipparcos* average main sequence as defined by Wright (2005).

Using the SME (Spectroscopy Made Easy) LTE spectral synthesis code (Valenti & Fischer 2005), we analyzed two high-resolution, iodine-free Keck-HIRES spectra of HD 156668 and found the effective temperature, surface gravity, projected rotational velocity, and iron

abundance ratio listed in Table 1. The errors on these four quantities have been conservatively doubled from the formal SME parameter uncertainties because the stellar atmosphere models are less certain at low T_{eff} (the SME catalog (Valenti & Fischer 2005) models stars down to $T_{\text{eff}} = 4800$ K). We refined the above parameters and derived stellar mass, radius, and luminosity from SME and interpolated Yonsei-Yale (Y^2) isochrones (Demarque et al. 2004) using an iterative process that self-consistently ties together the SME and Y^2 values of $\log g$ (Valenti et al. 2009). HD 156668 appears to be a typical middle-aged K dwarf. Its slightly super-solar iron abundance of $[\text{Fe}/\text{H}] = +0.05 \pm 0.06$ is consistent with its location near the average main sequence.

Measurements of the cores of the Ca II H & K lines show that HD 156668 has modest chromospheric activity (Fig. 1). We measured the chromospheric activity indices $S_{\text{HK}} = 0.23$ and $\log R'_{\text{HK}} = -4.98$ using the method described Wright et al. (2004) and Isaacson & Fischer (2009). The full set of S_{HK} measurements for all observations of HD 156668 does not show a periodicity near the planet’s orbital of 4.6455 d (see § 5.3 for additional discussion).

We estimate a rotation period $P_{\text{rot}} \sim 48$ d using R'_{HK} and $B - V$ calibration (Noyes et al. 1984), which is consistent with the 51.5 d period measured by APT photometry (see § 5.2). Following Wright (2005), and based on the values of S_{HK} , M_V , and $B - V$, we estimate an RV jitter of 1.5 m s^{-1} . This empirical estimate is based on an ensemble of stars with similar characteristics and accounts for RV variability due to rotational modulation of stellar surface features, stellar pulsation, undetected planets, and uncorrected systematic errors in the velocity reduction (Saar et al. 1998; Wright 2005). As explained in § 4, jitter is added in quadrature to the RV measurement uncertainties for Keplerian fitting.

HD 156668 has several important characteristics that make it a nearly ideal RV target star. Like other old, chromospherically quiet stars with spectral types from late G to early K, HD 156668 appears to be near the minimum of astrophysical jitter arising from acoustic oscillations, granulation, and photospheric activity (see § 5.3 and Figure 7). The star is relatively bright, yielding high signal-to-noise spectra in ~ 4 –5 minutes per observation.

3. HIRES OBSERVATIONS AND DOPPLER REDUCTION

We observed HD 156668 with the HIRES echelle spectrometer (Vogt et al. 1994) on the 10-m Keck I telescope. The 107 observations span five years (2005–2009) with high-cadence observations—clusters of observations on 6–12 consecutive nights—beginning in 2007. All observations were made with an iodine cell mounted directly in front of the spectrometer entrance slit. The dense set of molecular absorption lines imprinted on the stellar spectra provide a robust wavelength fiducial against which Doppler shifts are measured, as well as strong constraints on the shape of the spectrometer instrumental profile at the time of each observation (Marcy & Butler 1992; Valenti et al. 1995).

We measured the Doppler shift from each star-times-iodine spectrum using a modeling procedure modified from the method described by Butler et al. (1996). The most significant modification is the way we model the intrinsic stellar spectrum, which serves as a reference point

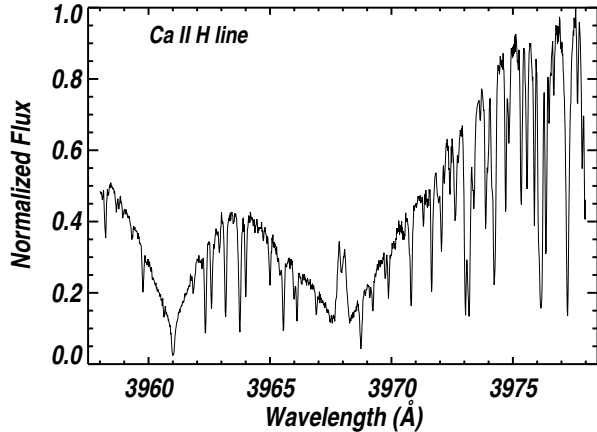


FIG. 1.— Ca II H line for HD 156668 from a Keck/HIRES spectrum. The line core emission near 3968 Å indicates modest chromospheric activity.

for the relative Doppler shift measurements for each observation. Butler et al. use a version of the Jansson (1995) deconvolution algorithm to remove the spectrometer’s instrumental profile from an iodine-free template spectrum. We instead use a new deconvolution algorithm developed by one of us (J. A. J.) that employs a more effective regularization scheme, which results in significantly less noise amplification and improved Doppler precision.

Figure 2 shows RV time series for four stable stars with characteristics similar to HD 156668, demonstrating our measurement precision of $\sim 1.5\text{--}2.0\text{ m s}^{-1}$ (including astrophysical, instrumental/systematic, and photon-limited errors) for chromospherically quiet late G/early K stars over the past 5 years. All of the measurements reported here were made after the HIRES CCD upgrade in 2004 August and do not suffer from the higher noise and systematic errors that limited the precision of pre-upgrade measurements to $\sim 2\text{--}3\text{ m s}^{-1}$ for most stars.

The velocities derived from the 107 observations have a median single measurement uncertainty of 1.01 m s^{-1} . This uncertainty is the weighted standard deviation of the mean of the velocity measured from each of the $\sim 700\text{ }2\text{ Å}$ chunks in each echelle spectrum (Butler et al. 1996). In a few cases, we made consecutive observations of HD 156668 to reduce the Poisson noise from photon statistics. For the Keplerian orbital analysis below (§ 4), the velocities were binned in 2 hr intervals, yielding 86 measurements with an rms of 2.71 m s^{-1} about the mean and a median measurement uncertainty of 0.99 m s^{-1} .

4. ORBITAL ANALYSIS

The measured radial velocities of HD 156668 are listed in Table 3 and plotted as a time series in Figure 3a. Before any fitting or filtering, these velocities already have a low rms, $\sigma = 2.71\text{ m s}^{-1}$. However, long-term trends, coherent over at least several months, are apparent by visual inspection of Figure 3a (see, e.g., the downward trend in 2007). These trends manifest themselves in a Lomb-Scargle periodogram (Lomb 1976; Scargle 1982) of the data as long-period power concentrated near $\sim 2.3\text{ yr}$ (Figure 3e).

The RVs also show a significant periodicity near 4.647 d

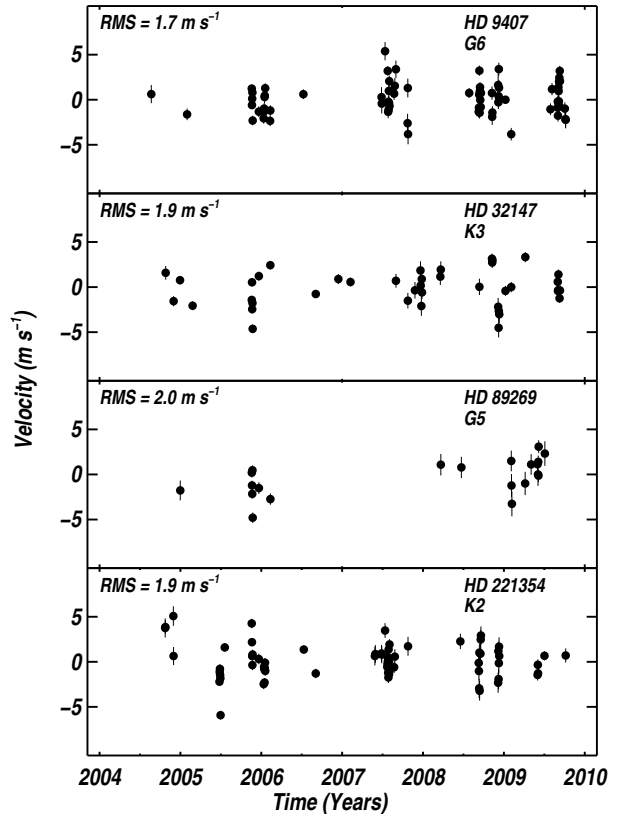


FIG. 2.— Radial velocity time series for four stable stars in our Keck Doppler survey that are similar to HD 156668. These stars demonstrate long-term velocity stability and precision of HIRES. The binned velocities with measurement uncertainties (but not jitter) are plotted. Panels are labeled with star name, spectral type, and velocity rms.

with power than exceeds the 0.1% FAP threshold¹⁰. A second short-period peak is visible at 1.270 d, but this peak is a stroboscopic alias of the 4.647 d signal with the sidereal day length (see § 5.4). We attempted to fit the radial velocities with a single-planet Keplerian orbital solution seeded with $P = 4.647\text{ d}$ using a partially-linearized, least-squares fitting procedure (Wright & Howard 2009). Each velocity measurement was assigned a weight constructed from the quadrature sum of the measurement uncertainty (listed in Table 3) and a stellar jitter term (1.5 m s^{-1}). The fitting routine converged on a robust solution with $P = 4.6455\text{ d}$, $e = 0.39$, and $K = 2.28\text{ m s}^{-1}$. This model gives $\sigma = 2.33\text{ m s}^{-1}$ and $\chi_\nu = 1.70$, a significant improvement over a linear model to the data.

We also tried fitting the long-period signal with a single-planet Keplerian model. We seeded the fitting routine with a range of periods and found a best-fit solution with $P = 791\text{ d}$ (2.17 yr) and a poorly constrained eccentricity when that parameter is allowed to float. The im-

¹⁰ The false alarm probability (FAP) thresholds plotted as dashed horizontal lines in the periodograms in Figure 3 refer to the probability that periodograms of random rearrangements of the data would exceed the specified power level. Since periodograms only measure the power of sine wave fits to the data (i.e. circular orbits), these FAPs are less conservative than the ones described in § 5.1 that allow for eccentric orbits and use the $\Delta\chi_\nu^2$ statistic.

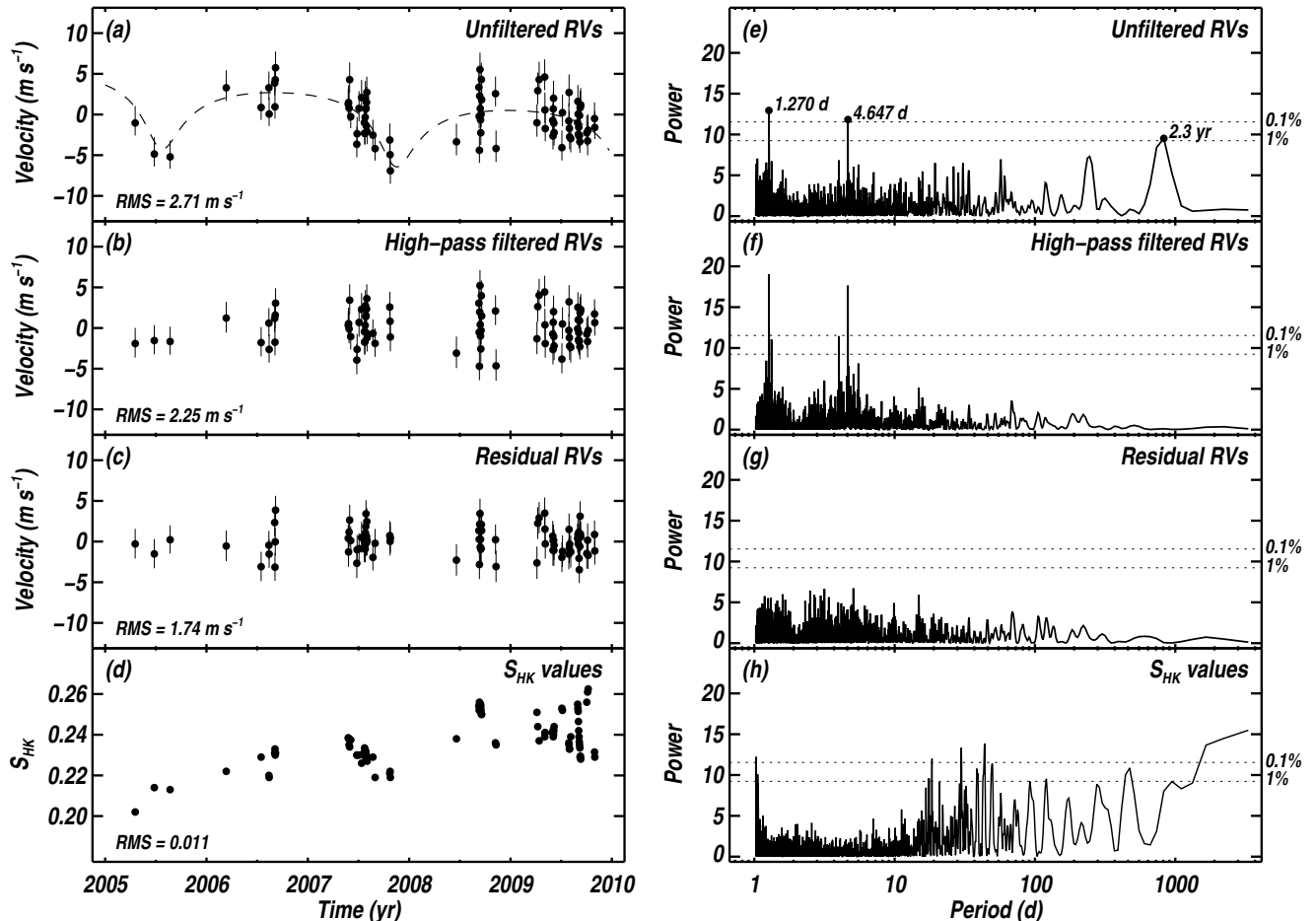


FIG. 3.— RV measurements and S_{HK} values for HD 156668 based on Keck-HIRES spectra. Each pair of panels in a given row displays the same data as a time series (panels *a–d*, on left) and as a periodogram (panels *e–g*, on right). Panels *a* and *e* show the unfiltered RVs from Table 3 with significant Fourier power at ~ 2.3 yr, 4.647 d, and 1.270 d (an alias of 4.647 d with the sidereal day length). Panels *b* and *f* show the RVs after applying a high-pass filter by subtracting the dashed line model in panel *a*; note that the ~ 2.3 yr signal was almost completely removed, strengthening the power at 4.647 d and its aliases. Panels *c* and *g* show the residuals of the high-pass filtered data to a one-planet fit with $P = 4.6455$ d in a circular orbit. Panels *d* and *h* show values of the chromospheric index S_{HK} derived from each RV measurement.

improvements in σ and χ_ν for this model are comparable to those from the $P = 4.6455$ d model described above. However, the poorly constrained and high eccentricity of the fit and the uneven phase coverage render the interpretation of this signal suspect. We cannot be sure if it is due to a planet in Keplerian motion, an astrophysical signal such as chromospheric activity masquerading as a RV change of the star, or some other effect.

Whatever the *source* of the long-period signal, its *effect* is to obscure the short-period signal. We considered several ways to high-pass filter the RVs to isolate the short-period signal. A key requirement of such a filtering process is that it leave the short-period signal untouched. We concluded that fitting the data to a two-planet model plus a linear trend would robustly separate the long and short-period signals, allowing for accurate parameter estimation for the short-period signal and a fair assessment of its statistical significance. The fitting routine converged on a robust solution with Keplerian parameters for the inner planet listed in Table 2. We adopt these parameters for HD 156668b. The “outer planet” in this model has $P = 2.31$ yr, $e = 0.48$, $K = 4.05$ m s $^{-1}$, $\omega = 178$ deg,

TABLE 2
ORBITAL SOLUTION FOR HD 156668 B

Parameter	Value
P (days)	4.6455 ± 0.0011
T_c (JD - 2,440,000)	14718.57 ± 0.11
e	$\equiv 0.0$
K (m s $^{-1}$)	1.89 ± 0.26
$M \sin i$ (M_\oplus)	4.15 ± 0.58
a (AU)	0.0500 ± 0.0007
N_{obs} (binned)	86
Median binned uncertainty (m s $^{-1}$)	0.99
Assumed jitter (m s $^{-1}$)	1.50
σ (m s $^{-1}$)	1.74
$\sqrt{\chi_\nu^2}$	0.97

$T_p = 2,454,414.22$, and $dv/dt = 0.94$ m s $^{-1}$ yr $^{-1}$ as shown by the dashed line in Figure 3. We emphasize that the outer planet in this fit is only a convenient model for the data, effectively serving as a high-pass filter to isolate the signal of the inner planet. Determining whether the long-period signal represents a planet will require additional RV measurements and diagnostic data.

Figure 3b/f shows the RV measurements after subtracting the long-period signal. Trends in the time series are no longer apparent and the 4.647 d signal and its alias at 1.270 d are significantly strengthened in the periodogram. Figure 3c/g shows the RVs after subtracting both long and short period signals. The value of σ is 1.74 m s^{-1} and the periodogram appears nearly featureless, with no periods remaining having significant power.

The phased orbital solution for HD 156668 b is shown in Figure 4. The Doppler semi-amplitude of $K = 1.89 \text{ m s}^{-1}$ is extremely low and is nearly equal to the 1.80 m s^{-1} typical error for single measurements (including jitter). The resulting minimum mass of $M \sin i = 4.15 M_{\oplus}$ is also extremely small, and is the second lowest reported to date using the RV technique. We adopted a circular orbit because the uncertainty on the eccentricity ($e = 0.20 \pm 0.17$) is significant when that parameter is allowed to float in the two-planet fit. Further, the best-fit eccentric orbit model did not show a statistically significant improvement in χ_{ν} compared to the circular orbit model.

The Keplerian parameter uncertainties were derived using a Monte Carlo method (Marcy et al. 2005). The uncertainty estimates on $M \sin i$ and a account for the uncertainty from M_{\star} . With five years of observations of this short-period planet, the error on P is quite small (one part in 4000).

5. THE NULL HYPOTHESIS

In this section we explicitly consider the null hypothesis. That is, we consider whether the $P = 4.6455$ d signal we identified as due to a low-mass planet in Keplerian motion could be due to another source. Such an analysis is motivated by the extremely low amplitude signal ($K = 1.89 \text{ m s}^{-1}$) and because of the use of high-pass filtering.

5.1. False Alarm Probabilities

We considered the possibility that the $P = 4.6455$ d signal arose from the chance arrangement of random, statistically independent errors in the RVs by computing FAPs for several fits to the data (Marcy et al. 2005; Cumming 2004; Howard et al. 2009a,b). These FAPs compare the measured data to 1000 scrambled data sets drawn randomly with replacement from unscrambled data. For each data set we compare a best-fit Keplerian model to the null hypothesis (a linear fit to the data) by computing $\Delta\chi_{\nu}^2 = \chi_{\text{lin},\nu}^2 - \chi_{\text{Kep},\nu}^2$, where $\chi_{\text{lin},\nu}^2$ and $\chi_{\text{Kep},\nu}^2$ are the values of χ_{ν}^2 for linear and Keplerian fits to the data, respectively. The $\Delta\chi_{\nu}^2$ statistic measures the improvement in the fit of a Keplerian model compared to a linear model of the same data. The FAP is the fraction of scrambled data sets that have a larger value of $\Delta\chi_{\nu}^2$ than for the unscrambled data set. That is, the FAP measures the fraction of scrambled data sets where the improvement in $\Delta\chi_{\nu}^2$ from a best-fit Keplerian model over a linear model is greater than the improvement of a Keplerian model over a linear model for the actual measured velocities. We use $\Delta\chi_{\nu}^2$ as the goodness-of-fit statistic, instead of other measures such as χ_{ν} for a Keplerian fit, to account for the fact that the scrambled data sets, drawn from the original velocities *with replacement*, have different variances, which sometimes artificially improve the

fit quality (i.e. some scrambled data sets contain fewer outlier velocities and have lower rms). Note that this FAP does not measure the probability of non-planetary sources of true velocity variation masquerading as a planetary signature.

We computed an FAP for the “two-planet model” (with the long-period planet acting as a high-pass filter) by comparing $\Delta\chi_{\nu}^2$ for the actual data with $\Delta\chi_{\nu}^2$ for two-planet fits to scrambled sets of the high-pass filtered data with the unscrambled long-period signal added back in. This FAP has a value of 0.3% (3/1000) and tests whether the statistical significance of the short-period signal is somehow enhanced by simultaneously fitting for a long-period signal.

We also computed the FAP for a 1-planet fit to the high-pass filtered data. We compared $\Delta\chi_{\nu}^2$ for the unscrambled, filtered data set and scrambled versions thereof. This FAP tests whether the short-period signal is a statistical fluctuation, while assuming that the long-period signal is real (but still of unknown origin). We found an FAP of 0.4% (4/1000) for this scenario (with eccentricity unrestricted in the fits to scrambled data sets). We note that *all* four of the false alarm solutions had best-fit parameters that appeared unphysical: high eccentricity ($e > 0.5$) and short period ($P < 10$ d). (We regard them as unphysical because short-period planets are almost universally in near circular orbits.) Such spurious, high eccentricity solutions often appear as the best-fit solution to low rms RV data lacking a coherent signal. When we restricted the fits of scrambled data sets to circular orbits (as we did with the actual measurements), the FAP dropped to $< 0.1\%$ (0/1000).

We conclude that the $P = 4.6455$ d signal is statistically significant. Considering all of the FAP tests, we estimate that the probability that this signal arose just due to random errors is less than 1% and probably on the order of 0.1%.

5.2. Photometric Observations

In addition to the Keck RVs, we obtained contemporaneous Strömgren b and y photometric measurements with the T10 0.80 m automatic photometric telescope (APT) at Fairborn Observatory in Arizona. This APT is identical to the T8 APT that was used to acquire photometric observations of HD 7924 in the first paper of this series (Howard et al. 2009b). (That paper mistakenly identified the APT used as the T12 0.8 m APT.) Our observing procedures and data reduction procedures in this paper are identical to those described in Howard et al. (2009b).

Our three comparison stars A, B, and C for HD 156668 (star D) were HD 158974 ($V = 5.63$, $B - V = 0.96$, G8 III), HD 155092 ($V = 7.07$, $B - V = 0.42$, F2), and HD 156536 ($V = 7.51$, $B - V = 0.42$, F3 IV), respectively. The T10 APT acquired 477 good observations of this quartet of stars covering the 2007, 2008, and 2009 observing seasons. Comparison star A, HD 158974, exhibits low-amplitude brightness variability of 5 mmag with a period of 152 days. The $C - B$ differential magnitudes have a standard deviation of 1.7 mmag, indicating that both stars are constant to the level of our measurement precision. Therefore, we created differential magnitudes of HD 156668 by averaging the $D - B$ and $D - C$ differential magnitudes into a single $D - (B + C)/2$ differential magnitude to be used for our analyses. We also combined

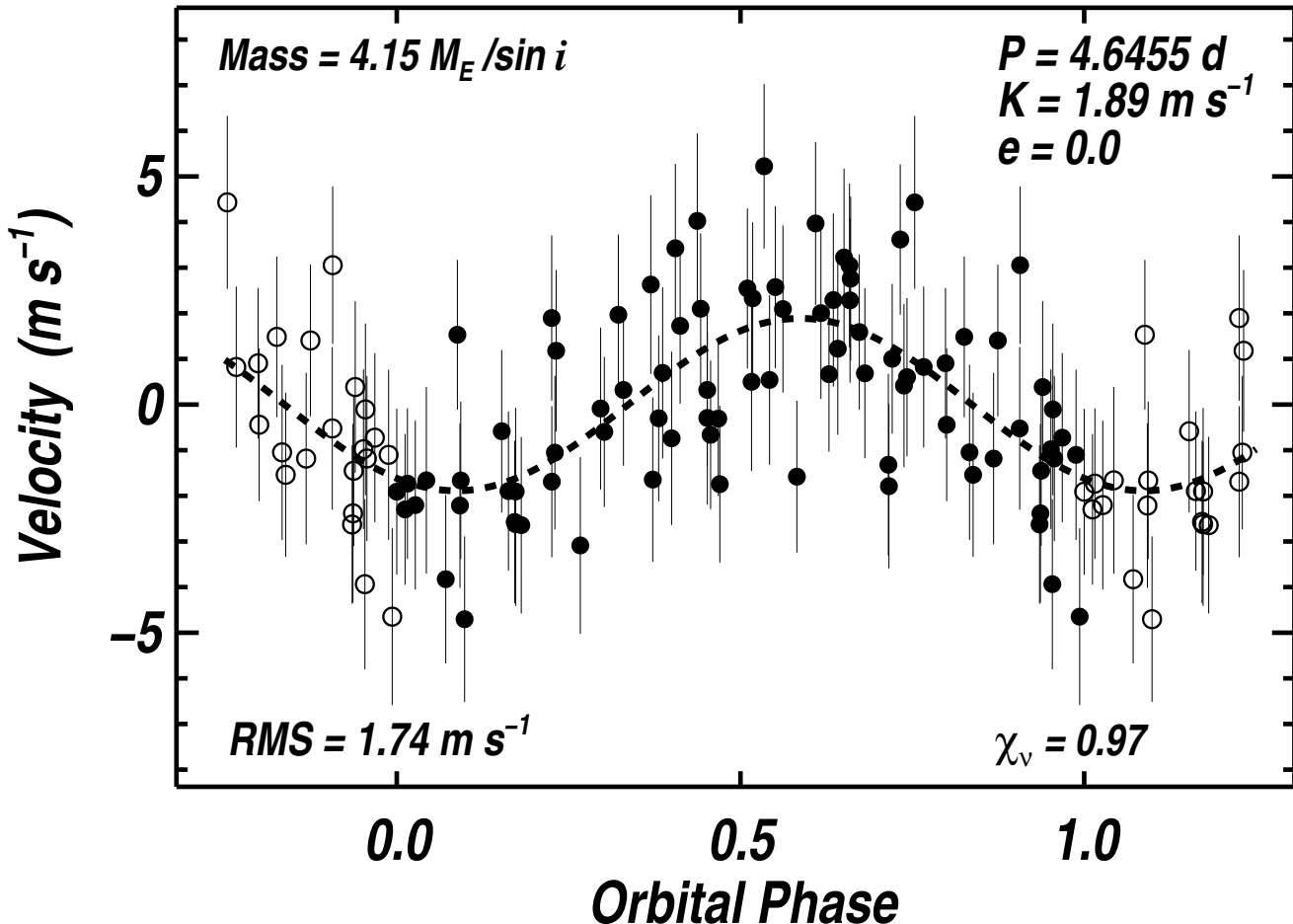


FIG. 4.— Single-planet model for the radial velocities of HD 156668, as measured by Keck-HIRES. The dashed line shows the best-fit circular orbital solution representing a $4.15 M_{\oplus}$ (minimum mass) planet in a 4.6455 d orbit. Filled circles represent phased, binned, and high-pass filtered velocities, while the open circles represent the same velocities wrapped one orbital phase. The error bars show the quadrature sum of measurement uncertainties and 1.5 m s^{-1} jitter.

our b and y observations into a single $(b+y)/2$ passband to improve the precision further.

These $D - (B+C)/2$ magnitudes in the $(b+y)/2$ passband are shown in the top panel of Figure 5. The gaps following the longer runs of data are due to the necessity of shutting down APT operations during the summer rainy season in Arizona. The gaps following the shorter data groups are the normal seasonal gaps for HD 156668. A summary of the photometric observations is given in Table 3. Column 5 indicates that the seasonal mean magnitudes vary over a range of ~ 1 mmag, which is typical for solar-type stars with modest chromospheric activity (see, e.g., Lockwood et al. 2007).

The vertical bars in the top panel of Figure 5 encompass the portion of the $D - (B+C)/2$ light curve that most clearly exhibits coherent variability that might be due to rotational modulation of spots on the star’s photosphere (see, e.g., Henry et al. 1995). That section of the light curve is replotted in the second panel. Straight line segments approximate the 2.5 cycles of the purported brightness variability.

Plotted in the third panel of Figure 5 is the frequency spectrum of the observations from panel two, showing a clear periodicity of 51.5 d. In the bottom panel, the same observations are phased to the 51.5 d period and a time

of minimum computed with a least-squares sine fit to the observations. The sine fit also gives a peak-to-peak amplitude of 2.3 ± 0.3 mmag.

We take the 51.5 d period to be the rotation period of HD 156668. This is consistent with $v \sin i = 0.5 \text{ km s}^{-1}$ and is very close to the rotation period of 48 d predicted from its level of chromospheric activity.

The APT photometry is also useful for confirming that observed RV variations are due to a planetary companion and not stellar surface activity. Queloz et al. (2001) and Paulson et al. (2005) have demonstrated how rotational modulation in the visibility of star spots on active stars can result in periodic RV variations and their misinterpretation. All 477 photometric observations of HD 156668 are plotted in the top panel of Figure 6, phased with the 4.6455 d RV period and a time of mid-transit computed from the orbital elements. A least-squares sine fit on that period gives a semi-amplitude of only 0.10 ± 0.11 mmag. This absence of detectable rotational modulation of surface activity to high precision on the RV period provides strong evidence that the RV variations arise from a super-Earth companion.

The bottom panel of Figure 6 replots the photometric observations that lie near the predicted time of transit. The solid curve shows the predicted depth (3.1 mmag)

TABLE 1
SUMMARY OF PHOTOMETRIC OBSERVATIONS OF HD 156668

Observing Season (1)	N_{obs} (2)	Date Range (HJD - 2,400,000) (3)	Sigma (mag) (4)	Seasonal Mean (mag) (5)
2007	181	54117–54407	0.00195	1.27046 ± 0.00014
2008	225	54484–54754	0.00188	1.27121 ± 0.00013
2009	71	54865–55004	0.00131	1.27013 ± 0.00016

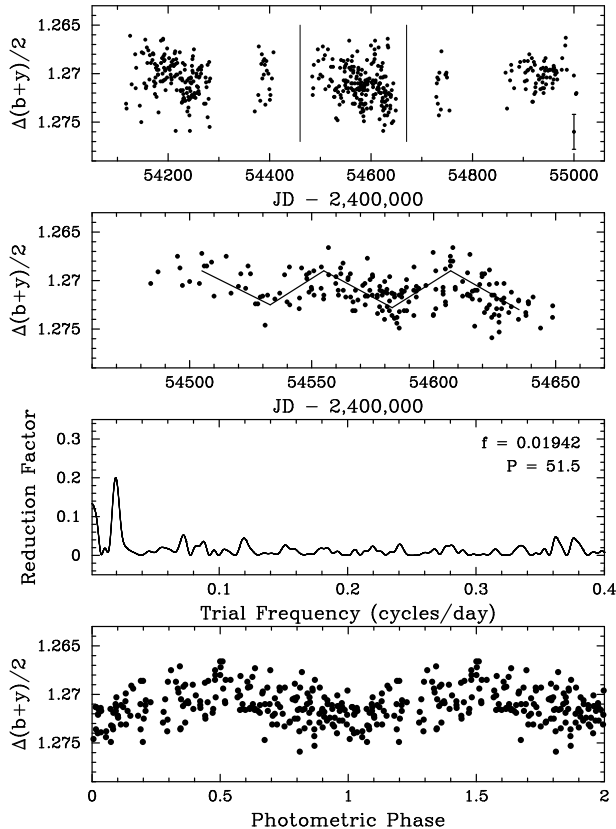


FIG. 5.— *Top*: The 477 $D - (B + C)/2$ photometric observations of HD 156668 in the $(b + y)/2$ passband, acquired with the T10 0.8 m APT during the 2007, 2008, and 2009 observing seasons. *Second panel*: The portion of the 2008 observing season set off by vertical bars in the top panel shows the most coherent brightness variability due to cool star spots carried across the disk of the star by its rotation. *Third panel*: Frequency spectrum of the observations in the second panel gives a best period of 51.5 days. *Bottom Panel*: Plot of the data from panel two phased with the 51.5-day period reveals coherent variability with a peak-to-peak brightness amplitude 0.0023 mag.

and duration (± 0.011 phase units) of a central transit, computed from the orbital elements and stellar properties with an assumed planetary composition of pure hydrogen. That such shallow transits can be detected with the APTs has been shown by Sato et al. (2005), who used the T11 APT to discover the 3 mmag transits of HD 149026b. The dotted line across the transit window corresponds to the expected depth (0.6 mag) of a hypothetical planet composed of entirely water. Our observations show that transits with a depth of 3.1 mag probably do not occur, essentially ruling out transits of a hydrogen planet. Additional precise photometry is required to rule out other planetary compositions.

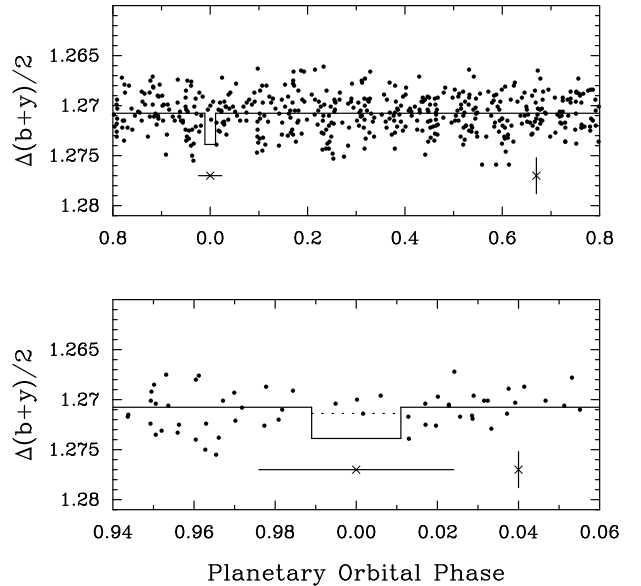


FIG. 6.— *Top panel*: The 477 APT photometric observations of HD 156668 plotted modulo the 4.6455 d period of the RV variations. A least-squares sine fit at that period yields a semi-amplitude of only 0.10 ± 0.11 mmag, providing strong evidence that the velocity variations arise from a planetary companion. *Bottom panel*: The photometric observations of HD 156668 near the predicted time of transit replotted with an expanded scale. The solid curve shows the predicted depth (3.1 mmag) and duration (± 0.011 phase units) of a central transit, computed from the orbital elements, the stellar properties, and a planetary composition of pure hydrogen. The uncertainty in the predicted transit time is shown by the error bar under the transit window. The dotted line across the transit window shows the expected depth (0.6 mmag) for a planet composed of water. Transits of a pure hydrogen planet are essentially ruled out. Additional observations are required to rule out other planetary compositions.

5.3. Chromospheric Activity

RV planet searches measure the shifts of the centroids of thousands of stellar lines. The shapes of individual lines are determined in large part by Doppler broadening from the disk-averaged velocity field of the star's surface. Spots are magnetically-controlled regions of the stellar photosphere characterized by temperatures ~ 1000 K lower than unaffected regions. As they rotate across the stellar surface, spots contribute less flux to particular parts of each absorption line profile—less flux on the blue side of lines for spots on the approaching limb and less flux on the red side for spots on the receding limb—thereby distorting the average line profile, shifting the centroid, and causing an apparent Doppler shift of the star.

False positive signals of this type tend to occur around chromospherically active stars (Queloz et al. 2001; Paulson et al. 2005). The spurious RV signals are

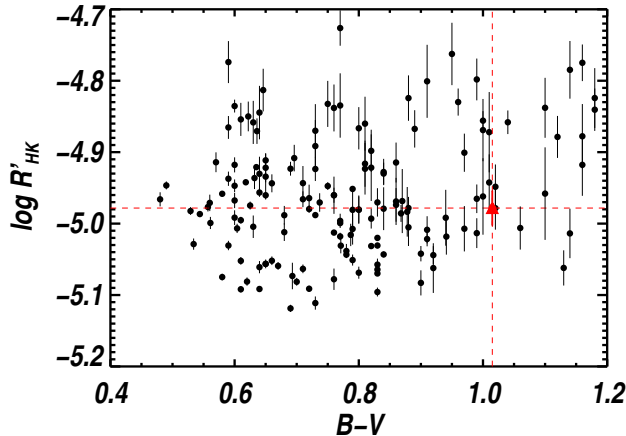


FIG. 7.— Plot of $\log R'_{\text{HK}}$ as a function of $B - V$ color for all G and K stars in the Eta-Earth survey with $B - V < 1.2$. HD 156668 (large red triangle highlighted by dashed red lines) is among the least chromospherically active Eta-Earth stars with similar $B - V$.

coherent over typical spot lifetimes (weeks to months) and have periods similar to the stellar rotation period. In § 5.2 we showed that the 4.6455 d signal is not seen in APT photometry, ruling out rotationally modulated spots as the source of the RV periodicity. Here, we use the chromospheric indices S_{HK} and $\log R'_{\text{HK}}$ to strengthen that conclusion further. These indices measure the level of stellar chromospheric activity, which in turn is strongly correlated with the magnetic activity of the stellar photosphere.

Some stars also show long-term chromospheric activity cycles as the average number of spots rises and falls with the solar cycle, typically with a timescale of ~ 10 yr. These cycles are sometimes detected as apparent RV shifts and incorrectly interpreted as long-period planets.

Figure 7 shows the average value of $\log R'_{\text{HK}}$ for HD 156668 and the other stars in the Eta-Earth Survey with $B - V < 1.2$. HD 156668 is among the least chromospherically active stars of similar spectral type in the Eta-Earth Survey. This is consistent with our limits on photometric variability from APT measurements (§ 5.2) and the small RV residuals to the Keplerian fit.

The values of S_{HK} derived from each Keck-HIRES spectrum are listed in Table 3 and plotted as a time series in Figure 3d. A Lomb-Scargle periodogram of the data is plotted in Figure 3h. Importantly, the periodogram shows negligible power for $P \lesssim 20$ d, as expected for a middle-aged star with a predicted rotation period of ~ 48 d. This lack of power at periods near 4.6 d strengthens the case for HD 156668 b.

On average, S_{HK} rises with time (Figure 3d), possibly due to the observation of a partial solar magnetic cycle. This several year long trend is not observed in the RVs (Figure 3a). One feature of the RV time series is also apparent in the S_{HK} , the declining trend in late 2007. This apparent correlation raises the possibility that the long-period signal that was filtered out of the RVs in § 4 is due to stellar activity. Despite this apparent correlation, the Pearson linear correlation coefficient, $r = +0.11$, between the unfiltered RVs and the S_{HK} values indicates an insignificant correlation. When we subtract a second-order polynomial fit to the S_{HK} values, the correlation

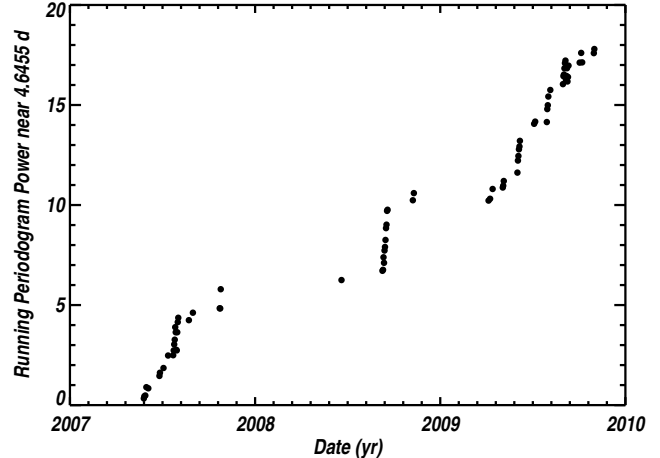


FIG. 8.— Running periodogram power near $P = 4.6455$ d as a function of time. Each dot represents the maximum periodogram power for the set of all high-pass filtered RVs up to that point in time. Only periods near the orbital period of HD 156668 b ($P = 4.64\text{--}4.65$ d) were used to compute each maximum periodogram power value. The monotonic rise confirms that the signal was present throughout the observations and points to a dynamical origin.

with the RVs is still statistically insignificant, $r = +0.19$. Thus, the suggestion that stellar activity explains the long-period signal is not well supported when the entire data set is considered.

Rotational modulation of spots and other surface features can also be detected in the spectral line bisectors (Torres et al. 2005). However, for this extremely low amplitude signal ($K < 2 \text{ m s}^{-1}$), detecting line profile variations at the same or higher precision is not possible.

As a final check, we show in Figure 8 that the RV signal from HD 156668 b is strictly periodic and present throughout the observations, as the clock-like signal from a planet should be. The plot shows the periodogram power of the planet rising monotonically as additional measurements are taken. False periodicities, such as those due to spots, typically exhibit periodicities that are only briefly coherent and that may reappear with slightly different periods.

5.4. Stroboscopic Alias

We interpret the periodogram spike near 1.270 d (Figure 3) as a stroboscopic alias of the orbital period (which appears on the periodogram as 4.647 d due to finite period sampling) with the sidereal day length (0.997 d): $1/4.647 \text{ d} + 1/1.270 \text{ d} = 1/0.997 \text{ d}$. We verified this by computing the periodograms of 2000 mock data sets that have the same times of observations and errors as the actual RVs. Of the 1000 data sets that we injected a 4.647 d signal, 851 of them showed significant periodogram power (≥ 10) near 1.27 d. Conversely, 0/1000 of the mock data sets with a 1.270 d signal added showed significant power near 4.647 d.

6. DISCUSSION

We present the detection of HD 156668 b, a super-Earth planet with minimum mass $M_P \sin i = 4.15 M_{\oplus}$ in a $P = 4.6455$ d orbit around a K3 dwarf. We draw on several lines of evidence to support the existence of HD 156668 b. We showed in § 5.1 that the short-period

signal is statistically significant. This signal is apparent in a fit to the unfiltered RVs, and stands out strongly when isolated by high-pass filtering. The host star is middle-aged and quiet, providing a nearly ideal RV target. The planet’s short-period signature is not seen in photometric observations or in chromospheric indices. Thus, the evidence strongly points to a planetary interpretation.

To estimate the orbital parameters of HD 156668 b, we found it necessary to apply a high-pass filter to the RVs by subtracting the model of a long-period Keplerian. This model changes slowly over time and clarifies, but does not artificially enhance, the $P = 4.6455$ d signal of HD 156668 b. Filtering of this type is common in other areas of time domain astronomy (e.g. transit photometry, astroseismology) and is uncommon, but not unprecedented, in RV planet detection. Similar filtering techniques were employed to disentangle the planetary signals of Gl 176 b (Forveille et al. 2009) and Gl 674 b (Bonfils et al. 2007), although in those cases the non-planetary signal was clearly due to spots modulated by stellar rotation. Queloz et al. (2009) used a “pre-whitening” technique to extract the signatures of two super-Earths from the complicated RV time series of the significantly more active star, Corot-7. Further, many exoplanets are announced with a model that includes a linear or second order RV trend, presumably due to a long period orbital companion. The source of the long-period signal remains unknown and motivates additional measurements. If it is due to a planet, the body has minimum mass $\sim 45 M_{\oplus}$ and orbits with $P_c = 2.31$ yr and $a_c = 1.6$ AU, a cold super-Neptune near the ice line.

We see no evidence for transits of HD 156668 b down to a level of ~ 3 mmag. However, given the large *a priori* transit probability of 7%, it is instructive to speculate about the transit signatures of various possible planet compositions. Using the models in Seager et al. (2007), a $4 M_{\oplus}$ planet composed of pure Fe, MgSiO_3 , H_2O , or H would yield planets of radius $R_{\text{pl}} = 1.2, 1.5, 2.0,$ and $4.5 R_{\oplus}$, producing transits of depth 0.22, 0.35, 0.61, and 3.1 mmag, respectively. These homogeneous planet models are oversimplified, but set the scale for admixtures of those ingredients: transits of planets made of solids and water would have depths of ~ 0.2 – 0.6 mmag, while transits of a planet with a significant atmosphere could be much deeper. For comparison, the transiting super-Earth Corot-7 b has a transit depth of 0.36 mmag implying a radius $R_{\text{pl}} = 1.68 R_{\oplus}$ (Léger et al. 2009). Using the RV-determined mass $M_{\text{pl}} = 4.8 M_{\oplus}$ (Queloz et al. 2009), the bulk density is terrestrial, $\rho_{\text{pl}} = 5.6 \text{ g cm}^{-3}$. In contrast, GJ 1214 b has $M_{\text{pl}} = 6.6 M_{\oplus}$ and $R_{\text{pl}} = 2.7 R_{\oplus}$, implying $\rho_{\text{pl}} = 1.9 \text{ g cm}^{-3}$, intermediate between Earth and the ice giants of the Solar System. Transits of GJ 1214 b are unusually deep (15 mmag) for a planet of this size because it orbits an M dwarf with $R_{\star} = 0.21 R_{\odot}$ (Charbonneau et al. 2009).

Several authors (e.g. Ida & Lin 2004, Mordasini et al. 2009) have argued that super-Earths will have insignificant hydrogen atmospheres (by mass) because during formation their masses failed to reach a critical mass (typically $\sim 10 M_{\oplus}$) when the growth from solid planetesimals is augmented by runaway accretion of gas from the protoplanetary disk. Smaller atmospheres (up to

several per cent by mass) could be produced by degassing during impact accretion and geological activity (Elkins-Tanton & Seager 2008; Kite et al. 2009). However, whatever atmosphere is acquired from these processes may be lost to atmospheric escape (Baraffe et al. 2006; Valencia et al. 2009). Nevertheless, the brief history of exoplanets is replete with observational surprises (hot Jupiters, eccentric orbits, etc.) so we consider the observational consequences of an atmosphere. Adams et al. (2008) find that adding a H/He gas envelope equivalent to 0.2–20% of the mass of a solid $5 M_{\oplus}$ exoplanet increases the radius 8–110% above the gas-free value. Atmospheres dominated by heavier molecules such as H_2O and N_2 (as on Earth) would swell the planet less for the same atmospheric mass because of the higher mean molecular weight and reduced scale height. Thus, we conclude that the APT photometric observations rule out transits for HD 156668 b if the radius is dominated by a H/He atmosphere (tens of per cent by mass), but do not preclude transits if the atmosphere is less massive or composed of heavier elements.

HD 156668 b adds statistical weight to the emerging trends of the properties of super-Earths and their hosts. Like most other such planets, it orbits a K or M dwarf. In contrast to other super-Earth hosts, HD 156668 has a slightly super-solar metallicity (Howard et al. 2009b). The rate of multiplicity in systems with super-Earths and Neptune-mass planets appears to be much higher than for higher mass planet hosts, with HD 40307 (Mayor et al. 2009a), GJ 581 (Mayor et al. 2009b), and HD 69830 (Lovis et al. 2006) being the standard examples of multiplicity in low-mass systems. The long-period signal seen for HD 156668 is suggestive of a second low-mass planet in the system.

HD 156668 b pushes the frontier of RV planet discovery to lower masses and smaller Doppler amplitudes. It is the second lowest minimum mass exoplanet discovered to date by the RV technique, after GJ 581 e (Mayor et al. 2009b). With a Doppler semi-amplitude of 1.89 m s^{-1} , HD 156668 b is also only the second exoplanet discovered to date with $K < 2.0 \text{ m s}^{-1}$. GJ 581 e is the other with $K = 1.85 \text{ m s}^{-1}$ and $M \sin i = 1.9 M_{\oplus}$ (Mayor et al. 2009b). This progress is remarkable: 51 Peg b was discovered (Mayor & Queloz 1995) with $M \sin i = 0.47 M_{\text{JUP}}$ and $K = 57 \text{ m s}^{-1}$ while the signal from HD 156668 b is smaller by factors of 35 and 30, respectively. However, we expect that true Earth analogs— $1 M_{\oplus}$ planets in 1 AU orbits around G stars—will remain permanently out of reach of the Doppler technique and will instead be discovered by transit photometry, astrometry, and microlensing. The Earth imparts a $K = 0.09 \text{ m s}^{-1}$ signal on the Sun, a factor of 20 smaller than HD 156668 b. Our Keck/HIRES observations of HD 156668 take ~ 5 min to achieve 1 m s^{-1} precision; scaling to 0.1 m s^{-1} precision requires 100 times the photons and impractically long integration times. (A handful of exceptionally bright nearby stars such as α Cen A/B may be an exception (Guedes et al. 2008).) Moreover, stellar jitter, even when averaged over with long integrations, likely limits Doppler precision to a few tenths of a m s^{-1} for the most quiet stars. Longer period planets suffer from the additional disadvantage that only a few orbits transpire during an observational campaign (com-

pared with ~ 100 orbits for the discoveries of HD 155668 b and GJ 581 e), reducing their detectability by clock-like coherence.

Nevertheless, the future of the Doppler technique is bright and we expect that it will continue to play a prominent role in planet searches. Discoveries of super-Earths and Neptunes from the Eta-Earth Survey will shape our understanding of planet formation and migration. Doppler work in other domains—long period giant planets, subgiants, multi-planet systems, dynamically interacting planets, Rossiter-McLaughlin measurements, etc.—will also continue to inform and enrich our knowledge of the rich astrophysics of exoplanets.

We thank the many observers who contributed to the velocities reported here. We gratefully acknowledge the efforts and dedication of the Keck Observatory staff, especially Scott Dahm, Hien Tran, and Grant Hill for support of HIRES and Greg Wirth for support of remote observing. We thank Heather Knutson, Doug Lin, Shigeru Ida, Jeff Scargle, and Ian Howard for helpful discussions. We are grateful to the time assignment

committees of the University of California, NASA, and NOAO for their generous allocations of observing time. Without their long-term commitment to RV monitoring, these long-period planets would likely remain unknown. We acknowledge R. Paul Butler and S. S. Vogt for many years of contributing to the data presented here. A. W. H. gratefully acknowledges support from a Townes Post-doctoral Fellowship at the U.C. Berkeley Space Sciences Laboratory. G. W. M. acknowledges NASA grant NNX06AH52G. G. W. H. acknowledges support from NASA, NSF, Tennessee State University, and the State of Tennessee through its Centers of Excellence program. This work made use of the SIMBAD database (operated at CDS, Strasbourg, France), NASA's Astrophysics Data System Bibliographic Services, and the NASA Star and Exoplanet Database (NStED). Finally, the authors wish to extend special thanks to those of Hawai'ian ancestry on whose sacred mountain of Mauna Kea we are privileged to be guests. Without their generous hospitality, the Keck observations presented herein would not have been possible.

REFERENCES

- Adams, E. R., Seager, S., & Elkins-Tanton, L. 2008, *ApJ*, 673, 1160
 Bakos, G. Á., et al. 2009, ArXiv e-prints
 Baraffe, I., Alibert, Y., Chabrier, G., & Benz, W. 2006, *A&A*, 450, 1221
 Beaulieu, J., et al. 2006, *Nature*, 439, 437
 Bennett, D. P., et al. 2008, *ApJ*, 684, 663
 Bonfils, X., et al. 2007, *A&A*, 474, 293
 Borucki, W. J., et al. 2009, *Science*, 325, 709
 Butler, R. P., Marcy, G. W., Williams, E., McCarthy, C., Dosanjuh, P., & Vogt, S. S. 1996, *PASP*, 108, 500
 Charbonneau, D., et al. 2009, *Nature*, 462, 891
 Cumming, A. 2004, *MNRAS*, 354, 1165
 Demarque, P., Woo, J., Kim, Y., & Yi, S. K. 2004, *ApJS*, 155, 667
 Elkins-Tanton, L. T., & Seager, S. 2008, *ApJ*, 685, 1237
 Forveille, T., et al. 2009, *A&A*, 493, 645
 Gray, R. O., Corbally, C. J., Garrison, R. F., McFadden, M. T., & Robinson, P. E. 2003, *AJ*, 126, 2048
 Guedes, J. M., Rivera, E. J., Davis, E., Laughlin, G., Quintana, E. V., & Fischer, D. A. 2008, *ApJ*, 679, 1582
 Henry, G. W., Fekel, F. C., & Hall, D. S. 1995, *AJ*, 110, 2926
 Høg, E., et al. 2000, *A&A*, 355, L27
 Howard, A. W., et al. 2009a, *ApJ*, submitted
 —. 2009b, *ApJ*, 696, 75
 Ida, S., & Lin, D. N. C. 2004, *ApJ*, 604, 388
 Isaacson, H. T., & Fischer, D. A. 2009, in preparation
 Jansson, P. 1995, *Deconvolution: With Applications in Spectroscopy* (Academic Press)
 Kite, E. S., Manga, M., & Gaidos, E. 2009, *ApJ*, 700, 1732
 Léger, A., et al. 2009, *A&A*, 506, 287
 Lockwood, G. W., Skiff, B. A., Henry, G. W., Henry, S., Radick, R. R., Baliunas, S. L., Donahue, R. A., & Soon, W. 2007, *ApJS*, 171, 260
 Lomb, N. R. 1976, *Ap&SS*, 39, 447
 Lovis, C., et al. 2006, *Nature*, 441, 305
 Marcy, G. W., & Butler, R. P. 1992, *PASP*, 104, 270
 Marcy, G. W., Butler, R. P., Vogt, S. S., Fischer, D. A., Henry, G. W., Laughlin, G., Wright, J. T., & Johnson, J. A. 2005, *ApJ*, 619, 570
 Mayor, M., & Queloz, D. 1995, *Nature*, 378, 355
 Mayor, M., et al. 2009a, *A&A*, 493, 639
 —. 2009b, *A&A*, 507, 487
 Mordasini, C., Alibert, Y., & Benz, W. 2009, *A&A*, 501, 1139
 Noyes, R. W., Hartmann, L. W., Baliunas, S. L., Duncan, D. K., & Vaughan, A. H. 1984, *ApJ*, 279, 763
 O'Toole, S., et al. 2009, *ApJ*, 697, 1263
 Paulson, D. B., Sneden, C., & Cochran, W. D. 2005, *AJ*, 130, 2436
 Queloz, D., et al. 2001, *A&A*, 379, 279
 —. 2009, *A&A*, 506, 303
 Saar, S. H., Butler, R. P., & Marcy, G. W. 1998, *ApJ*, 498, L153+
 Sato, B., et al. 2005, *ApJ*, 633, 465
 Scargle, J. D. 1982, *ApJ*, 263, 835
 Seager, S., Kuchner, M., Hier-Majumder, C. A., & Militzer, B. 2007, *ApJ*, 669, 1279
 Sumi, T., et al. 2009, ArXiv e-prints
 Torres, G., Konacki, M., Sasselov, D. D., & Jha, S. 2005, *ApJ*, 619, 558
 Unwin, S. C., et al. 2008, *PASP*, 120, 38
 Valencia, D., Ikoma, M., Guillot, T., & Nettelmann, N. 2009, ArXiv 0907.3067
 Valenti, J. A., Butler, R. P., & Marcy, G. W. 1995, *PASP*, 107, 966
 Valenti, J. A., & Fischer, D. A. 2005, *ApJS*, 159, 141
 Valenti, J. A., et al. 2009, *ApJ*, 702, 989
 van Leeuwen, F. 2007, *A&A*, 474, 653
 Vogt, S. S., et al. 1994, in *Proc. SPIE Instrumentation in Astronomy VIII*, David L. Crawford; Eric R. Craine; Eds., Vol. 2198, p. 362
 Wright, J. T. 2005, *PASP*, 117, 657
 Wright, J. T., & Howard, A. W. 2009, *ApJS*, 182, 205
 Wright, J. T., Marcy, G. W., Butler, R. P., & Vogt, S. S. 2004, *ApJS*, 152, 261

TABLE 3
 RADIAL VELOCITIES AND S_{HK} VALUES FOR HD 156668

JD - 2440000	Radial Velocity (m s^{-1})	Uncertainty (m s^{-1})	S_{HK}
13478.97768	-1.04	1.03	0.202

TABLE 3 — *Continued*

JD - 2440000	Radial Velocity (m s^{-1})	Uncertainty (m s^{-1})	S_{HK}
13547.90964	-4.86	0.99	0.214
13604.83890	-5.21	0.85	0.213
13807.14411	3.29	1.14	0.222
13932.91866	0.87	1.00	0.229
13960.91401	3.29	0.87	0.220
13961.80956	0.06	0.88	0.219
13981.77064	3.87	0.94	0.231
13982.87659	0.94	0.84	0.233
13983.81911	4.28	0.80	0.230
13984.90602	5.74	0.85	0.231
14247.01977	1.27	0.71	0.239
14248.00711	1.47	1.10	0.238
14249.92154	0.79	1.14	0.235
14252.01612	4.28	1.08	0.234
14255.84743	-0.27	0.76	0.238
14277.79111	-3.66	1.11	0.230
14278.80991	-2.37	0.98	0.230
14285.81562	0.75	1.10	0.230
14294.89361	2.08	1.16	0.226
14304.95027	-0.99	0.75	0.232
14305.95179	-2.31	0.69	0.234
14306.92739	-2.31	0.70	0.232
14307.97764	-0.33	0.73	0.231
14308.94701	2.07	1.00	0.229
14309.94163	0.68	0.71	0.232
14310.93496	0.77	0.66	0.230
14311.92755	-1.40	0.67	0.230
14312.93048	1.49	0.72	0.228
14313.92787	2.74	0.68	0.228
14314.96879	-2.10	1.01	0.227
14335.87372	-2.54	0.63	0.229
14343.79865	-4.20	0.89	0.219
14396.70306	-3.13	0.95	0.221
14397.70527	-4.94	0.93	0.222
14398.73491	-6.92	1.11	0.219
14636.95177	-3.36	1.23	0.238
14717.74461	3.34	0.99	0.254
14718.89500	-0.22	0.97	0.252
14719.78911	-4.40	1.02	0.256
14720.82821	2.28	0.92	0.255
14721.81321	5.53	1.00	0.255
14722.75844	0.73	0.97	0.255
14723.75113	-0.66	0.90	0.255
14724.77287	-2.25	0.96	0.254
14725.74632	0.03	1.03	0.252
14726.80657	4.30	0.97	0.250
14727.81096	1.82	0.92	0.250
14777.68651	2.56	1.05	0.236
14779.69190	-4.18	1.23	0.235
14927.05569	-1.01	1.31	0.251
14930.09564	2.92	1.26	0.244
14935.05529	4.30	1.19	0.237
14955.10678	4.61	1.16	0.239
14955.97159	0.56	1.14	0.241
14957.05565	-1.73	1.05	0.241
14983.97707	-0.72	1.09	0.241
14984.96665	-2.64	1.22	0.242
14985.92186	0.69	1.13	0.239
14986.99173	1.99	1.14	0.240
14987.99574	-1.07	1.20	0.242
14988.89618	-2.23	1.08	0.244
15016.97485	-4.08	1.08	0.253
15019.04148	0.23	1.25	0.252
15041.97022	-0.80	1.16	0.236
15042.89409	2.71	1.24	0.235
15043.90466	-1.71	1.13	0.233
15044.94394	-2.75	1.00	0.233
15048.86672	-2.97	1.26	0.239
15073.76736	-1.01	0.95	0.255
15074.75962	1.61	0.91	0.253
15075.73804	0.05	0.66	0.252
15076.74458	-2.42	0.68	0.247
15077.74489	-1.57	0.96	0.242
15078.76561	-2.64	1.00	0.239
15079.73946	-2.60	0.72	0.237
15080.74369	-0.13	0.69	0.235

TABLE 3 — *Continued*

JD - 2440000	Radial Velocity (m s^{-1})	Uncertainty (m s^{-1})	S_{HK}
15081.73701	-3.35	0.69	0.234
15082.72821	0.83	1.01	0.229
15083.73498	1.02	0.69	0.230
15084.74428	1.19	1.00	0.228
15106.76608	-2.26	1.16	0.256
15109.75425	-3.25	1.39	0.261
15111.72700	-1.94	0.79	0.263
15134.69674	-0.50	0.82	0.232
15135.70259	-1.59	0.80	0.229